



Behavior of Snow Containing an Ice Lens under Compressive Loading

Marin N. Blaisdell¹ and Ian Baker¹

¹Thayer School of Engineering, Dartmouth College, Hanover, NH 03755, U.S.A.

Correspondence to: Marin N. Blaisdell (marin.mnb@gmail.com)

Abstract. In order to understand the effects of strain rate on the mechanical response of snow containing an ice lens perpendicular to the loading direction, specimens with and without ice lenses were compressed at several different rates from 4 x 10⁻⁴ to 1.2 x 10⁻² s⁻¹. It was found that snow columns with an included ice lens follow the same behavior as homogeneous snow for the range of strain rates tested, the sole difference being a six-fold increase in stress at a given strain when an ice lens was present. For all samples, low strain rates (4 x 10⁻⁴ to 1.2 x 10⁻³ s⁻¹) resulted in a smooth steady increase in stress with increasing strain, whereas at high strain rates (4 x 10⁻³ to 1.2 x 10⁻² s⁻¹) two loading regimes occurred; up to ~20% strain the stresses increased minimally, while higher strains led to a more rapid stress increase. Snow columns both with and without an ice lens showed the highest resistance to loading at intermediate rates (2.1 x 10⁻³ to 3 x 10⁻³ s⁻¹) which allowed for reconfiguration of the ice particles whilst inducing pressure sintering to strengthen existing bonds. Stress differences between aged and fresh snow were distinct but not as large as those between ice lens-containing and homogenous snow, indicating that ice lenses have a higher contribution to snow strength than sintering alone.

1. Introduction

Avalanches are a significant cause of fatalities and economic damage in the alpine regions during the winter. Many studies have sought to understand and predict the initiation of avalanches to make life safer in avalanche prone areas (Schweizer et.al., 2003; LaChapelle 1977). A known instigator for avalanches is a horizon in the snowpack with low shear resistance. One common type of weak horizon is an ice layer, commonly called an ice lens due to its thinness compared to the overall snowpack.

Ice lenses often initially form on top of an existing deposit of snow. This ice can be formed from a melt-freeze event triggered by atmospheric temperature fluctuation, (Jamieson, 2006), strong solar gain (LaChapelle, 2011), or rain (Cohen et.al., 2015; Queno et.al., 2020). If additional snow is then deposited on the lens, the snowpack becomes a layered material with snow above and below the lens (Hammonds et.al., 2015). This configuration is usually highly unstable; the ice lens can act as a slip plane on which the above-lens snow can shear off the snowpack and trigger an avalanche (Schweizer, 1999). The behavior of a layered snowpack under load is important to understand to determine the conditions for slippage.

Although density is most often used to quantify snow for engineering purposes, it is wholly inadequate to assess strength. The mechanical properties of snow are affected by multiple phenomena; the characteristics and microstructure of falling snowflakes, time spent on or under existing snow, current and historical ambient temperatures, internal temperature gradient, and stratigraphy of the accumulated snowpack. Furthermore, a snowpack's strength can vary widely over timespans as short as 12 h. Early applied snow studies focused on the macroscopic behavior e.g. Abele, 1990. More recent research has significantly enhanced our understanding of snow's microstructure (see Baker, 2019 for a review) including in association with an embedded weak layer (Kochle et al., 2017).

A number of recent studies have attempted to relate microscopic behavior to macroscopic behavior (Wang and Baker, 2013; Hagenmuller et al., 2014c; Hagenmuller et al., 2015; De Biagia et al., 2019). These have resulted in increasingly close to



65



real-time observations of microstructure during and shortly after mechanical deformation of snow. The behavior of the crystals and bonds within the snow's ice-air matrix can now be observed using modern imaging techniques. The development of X-ray computed microtomography (MicroCT) has revolutionized how we visualize snow and has provided opportunities for observation of microstructural change. For instance, in Wang and Baker (2014), a MicroCT fitted with a compression stage was used to observe the effect of load on individual grains during compaction.

Experimental studies have utilized the MicroCT in tandem other methods to characterize and understand the behavior of snow under different loading conditions. Barraclough and others investigated the response of homogeneous dry snow (natural and artificial) to deformation, using DIC methods to visualize the strain behavior. They found that snow exhibits strain-rate softening: strong at low deformation rates where it is quasi-plastic, but weak at high rates where it becomes quasi-brittle. The team reports that snow can deform with the formation and propagation of localized deformation bands accompanied by oscillations of the driving force, concluding that strain localization can occur in initially homogeneous samples under homogeneous loads (Barraclough et al., 2017). Eppanapelli and others analyzed microstructural changes of dry natural snow during compaction using a MicroCT and DVC analysis to visualize displacement and strain fields. Results show that grains closest to the loading source experience the most displacement, and a distinct heterogeneity was observed in the porosity distribution in response to compaction 50 (Eppanapelli et al., 2019). In another experimental snow compaction study, Zheng subjected natural snow of different densities to varying rates of loading to propose new definitions of snow strength and deformation property parameters based on stress-strain curves. They provide detailed categorization of failure modes (ductile, brittle, and transitional) accompanied by corresponding descriptive equations for uniaxial compressive behavior (Zheng, 2024). Studying the relationship between macroscopic mechanical properties of snow and its microstructure, Ma and others used triaxial compression testing followed by MicroCT scans to observe changes in snow structure. They proposed a grain segmentation algorithm to relate stress-strain data to changes in the number and area of ice bonds. Results indicated that the snow loading process is split into two stages: initial loading and linear hardening, with the latter characterized by a significant decrease in ice bond area (Ma et al., 2025).

Buried ice lenses within a snowpack are of interest to avalanche researchers, and recent work has been done to better understand the susceptibility of weak layers to crack propagation, a primary mechanism of snow slab release. It should be noted that most studies are either aimed at modeling the behavior of depth or surface hoar, the most studied type of weak layer in snow, or use a generalized "weak layer" for modeling, assuming that the different types of heterogeneity that occur in a snowpack have the same response to crack propagation. However, the results could be applicable to the potentially vulnerable interface between snow and ice that a buried ice lens creates. To the author's knowledge there has not been extensive modeling work done on the predisposition of buried ice lenses specifically to crack propagation.

Gaume and others focused on the initiation of slab avalanches by using a finite-element code to build a mechanical model of the slab/weak-layer system. They represent the heterogeneous weak layers through Gaussian distributions of the cohesion and use stress redistribution from the slab elasticity as foundational variables. The system was loaded by increasing the slope angle until rupture, and several simulations were run for different configurations of heterogeneity of the weak layer. Results show a heterogeneity smoothing effect caused by slab elasticity (Gaume et al., 2013). Rosendahl and Weibgraeber proposed a closed-form analytical model for a snowpack under skier loading and a mixed-mode failure criterion for the nucleation of weak layer failure. The model provided deformations of the snow slab, weak layer stresses, and the energy release rates of cracks within the weak layer. The model was used to analyze propagation saw tests and the authors report that their computed weak layer fracture toughness values are in agreement with finite element analyses (Rosendahl and Weibgraeber, 2020). Experimental data on avalanche slab release is difficult to obtain but crucial for our understanding. In Jamieson's 2006 paper focused on the role of refrozen snowpack layers in slab release, he identified and characterized weak layers of faceted crystals that developed at the





interface between refrozen underlying wet layers (crusts) and the subsequently deposited surface snowpack. The interface is marked by differences in grain radii which contribute to weak bonding. Shear tests on facet layers showed an initial strength loss followed by a slow increase. He concludes that the processes that create ice crusts have a strong importance in determining the strength of the interface between the ice and surface snowpack (Jamieson, 2006). While the present study uses manufactured ice lenses not melt-freeze crusts, the concept that the weak bonding between ice and snow in shear contributes to slab release gives this work value to both the snow mechanics and avalanche research communities.

To the authors' knowledge, there are no studies which couple microstructural analysis with varying levels of mechanical deformation on heterogeneous snow columns. In this work, we subjected snow samples containing an embedded ice lens to compression testing at a range of strain rates and related the test results to observed changes in the microstructure. This work is directly applicable to snow and ice mechanics, and given the lack of available experimental data, could offer greater insight to the often complex interweb of components that constitute snow and ice behavior.

2. Methods

95

105

2.1. Sample Preparation

To create a laboratory version of a naturally-occurring ice lens-containing snowpack, a 25 mm diameter, 55 mm high transparent polycarbonate container was filled with natural snow and an ice lens. The natural snow was collected in Hanover, NH, with the majority of tests utilizing snow collected late in the winter of 2023-2024. This snow was stored in a -30°C cold room until testing took place in September 2024, when the snow was approximately eight months old. Fresh natural snow was collected again in late December 2024 offering a chance to compare its behavior with aged snow. This snow was also placed in a -30°C cold room and tested in early January 2025 when the snow was one month old.

As typical for mid-latitude seasonal snow, the grain type was dendritic, specifically the "Plane Crystal" type under the Magono and Lee (1966) classification system. A MicroCT was used to characterize the aged (8 mo) snow used in experiments: porosity was 70.8% with a standard deviation of 2.4% (equivalently the density was 268 kg/m³ +/- 2.2 kg/m³), and the specific surface area was 14.5 mm⁻¹ +/- 0.55 mm⁻¹. The fresh snow had a density of 225 kg/m³ calculated by mass over volume measurement. Due to equipment maintenance, a MicroCT analysis was not feasible for the fresh snow samples, so SSA data is not available for fresh snow. Comprehensive within-sample variability could not be obtained due to equipment and time limitations to be explained in following sections. Stored snow was first sieved to disaggregate the ice grains and then deposited into the sample containers. This procedure, accompanied with the sintering that occurred while the snow was held in storage, did appear to cause some grain metamorphism from highly dendritic (light and fluffy) to more rounded (harder and spherical) as indicated by the low SSA value.

The layered sample was completed by filling the container to the halfway mark with snow and gently tapping the container on a hard surface to level the snow and remove large air pockets. A manufactured ice lens was placed at the midpoint (27 mm from bottom) (Fig. 1). The ice lens was created from a cylindrical block of lab-grown granular ice. Using a precision band saw, the lens was cut from the block and adhered to a glass plate by heating, slightly melting the lens, then allowing the lens to freeze to the plate in the cold room. The lens was shaved to 2 mm thickness with a metal razor, removed from the glass plate, then shaped to size using the heated end of a 25 mm diameter thin-wall metal cylinder. The ice lens was left to cool and harden before being placed on top of the lower layer of snow in the sample container. The upper layer of snow was created in the same manner as the snow below the ice lens.







Figure 1. Ice lens sample. Snow was sieved into a 55 mm x 25 mm diameter container, and a 2 mm ice lens was situated midway with an approximately horizontal orientation.

This method limited the potential for large air pockets and, while such features can be found in naturally occurring snowpacks, for samples of a small size, uniformity was important to create replicable samples so that experiments could be accurately compared. This process did consolidate the snow but produced a uniform sample from which to compare before and after compression.

Experiments (imaging and compression) were performed both directly after sample preparation and 24 h after. The majority of tests were prepared and compressed the same day. There was no detectable difference in either the mechanical behavior or the microstructural between day-old and minute-old samples, so our parameter space only included snow age and ice lens presence as variables.

2.2. Experimental Design

Compression tests were performed at eight strain-rates for snow samples both with and without an ice lens. Layered snow samples were prepared in a cylindrical container with a manufactured ice lens placed at mid-height. A lifecycle or cradle-to-grave approach was used for testing; one prepared sample was analyzed from its initial uncompressed state to post-strain. Each round of experiments began with an initial MicroCT scan (before compression) to quantitatively characterize the unstrained snow. The sample was then moved to a MTS servo-hydraulic testing machine where it underwent compression testing at a range of strain rates from 4 x 10⁻⁴ s⁻¹ to 1.2 x 10⁻² s⁻¹ (displacement rates of 2.2 x 10⁻⁵ m.s⁻¹ to 6.6 x 10⁻⁴ m.s⁻¹). Test durations ranged from 30 s to 8 min. Both the MicroCT and MTS were located in cold rooms held at a temperature of -10°C. The rooms were separated by a walkway, so the transfer included a 15 s walk between rooms. This meant that the samples were exposed to room temperature air for that short period, the potential impacts of this on results are discussed in proceeding sections. After testing, the compressed sample was imaged again in the MicroCT to detect differences in the microstructure. Testing was performed to a total strain of 20%. It was found that greater than 20% strain caused the images produced by the MicroCT to be too similar since the compressed grains were too closely packed to see a discernible difference. However, we compressed many samples to 40% strain since the load-displacement behavior of the samples past 20% strain proved to be important. Samples that were tested to 40% strain were not imaged.

2.3. Compression Tests

140 2.3.1. Equipment and Set-up



145

155

160



Prepared samples were compressed in a MTS located in a -10°C cold room. It should be noted that some degree of "pre-loading" took place with every sample tested. This occurred when placing the plunger, which was not connected to the overhead resistance frame, directly on the snow surface during set-up. This minimally compressed the top-most portion of the snow sample. However, the displacement was observed to be small (1-2 mm) and since it was uniform for the entire test program, this was ignored.

The wood plunger fit snugly against the container walls yet could move freely; the gap measured 0.5 mm between the parts. This prevented snow from escaping compaction by moving up the sides, while simultaneously minimizing the friction between the plunger and container. The friction of the ice lens against the container walls had a similar resolution. While the ideal process for creating laboratory ice lenses was such that the diameters of the lens and container matched exactly, this was not the true diameter of the lens. Due to the slight melting of the edges, the true diameter of the lens was smaller than the container, leaving a gap the same size as the plunger-container distance (0.5 mm). Due to these experimental constraints, friction was reduced between both the plunger and the ice lens against the container. The friction was not completely negligible, however, any additional resistance due to friction of the lens and/or plunger against the container was consistent throughout this study and thus the samples can be accurately compared. Furthermore, the results of this study are aligned with other recent experimental studies of snow compaction (Zheng et al., 2024; Wang et al., 2021).

We used piston velocity, or a fixed displacement rate, as the independent variable with a chosen sample rate to yield approximately 2,000 measurements per test. These were calculated from the desired strain rates, total strain, and sample initial height. The test duration was calculated from these data, and the MTS was stopped at the corresponding time for each experiment to yield either 20% or 40% total strain. The total strain was selected based on whether post compaction MicroCT analysis would be performed.

Samples were tested at preset strain rates, and a digital acquisition system collected the load (N), displacement (mm), and time (s) data sets.

2.4. MicroCT Observations

2.4.1. Equipment and Set-up

Samples were imaged in a Skyscan 1172 MicroCT both before and after compression. Imaging was performed at an accelerating voltage of 40 kV, a current of 250 μ A, and an image pixel size of 16 μ m. Data generated from the MicroCT was used to calculate various microstructural parameters such as density, porosity, and specific surface area (SSA).

The scan region was centered on the snow-ice lens interface for a total scan height of 10 mm. A volume of interest (VOI) was created for each scan, above and below the lens, giving microstructural data for each region. Acquired images were subjected to post-processing analysis using the MicroCT-integrated software NRecon and CTAn. VOI cropped images were transformed to binary format by choosing a density threshold for which the software would distinguish phases (air and ice). This threshold was kept the same for all post-processing.

It should be noted that the small Field of View (FOV) of the MicroCT was a limiting factor in our analysis. We hoped to learn from these tests how loading changed the microstructure at, above, and below the ice lens surface. However, due to the small scanning FOV, we elected to focus on the ice lens' top face and the bulk snow properties just above the lens. A consequence of this was the inability to discern differences in microstructural values within a sample, further work should include analysis of these variables both above and below the ice lens to more comprehensively ascertain variability.

2.4.2. Data Analysis



180



Several quantities were generated by the MicroCT analysis software, but this study focused on two in particular: Specific Surface Area (SSA) and Connectivity Density (ConnD). These quantities are a general reflection of the degree of metamorphosis of the region; how connected the ice particles are, the amount/number of bonds, the strength of the bonds, and the grain size.

SSA is a measure of the complexity of structure. In general, it reflects the amount of bonding and structural metamorphosis the grains have undergone. Based on the hexahedral marching cubes method, SSA is defined as the surface-to-volume ratio, i.e. the snow surface divided by the snow volume. A high SSA indicates surface complexity, meaning that more surface area of snow is accessible to air. CTAn, the software calculating these values, includes "false" outside surfaces to be adjusted for. If the volume of interest (VOI) crops off an ice grain, it treats this edge as a surface. Therefore, we subtracted intersection surfaces from the total surface then divided by object volume for a more accurate value (Wang and Baker, 2014).

Connectivity Density, formally known as the Euler Number, is an indicator of connectedness of a 3D complex structure. It measures the degree to which parts of the object are multiply connected, i.e. how many connections in a structure can be severed before the structure falls into two separate pieces (Salmon, 2009). The calculation of ConnD is based on the Conneulor method developed by Odgaard (Gunderson et al., 1993). ConnD χ is determined by the Euler-Poincare formula (Eq. 1), where β_0 is the number of objects, β_1 is the connectivity, and β_2 is the number of enclosed cavities.

$$\chi(X) = \beta_0 - \beta_1 + \beta_2 \tag{1}$$

Euler analysis provides a measure of connectivity density, which can significantly contribute to structure strength (Odgaard, 1997).

When analyzing the SSA and ConnD data, an interesting phenomenon was discovered. The difference between pre and post compressed samples was within an acceptable margin of error when the samples tested were performed via a lifecycle method. When the samples were bulk tested –a different set of samples for pre and post compression –the difference between pre and post data sets was quite scattered and didn't show as clear a trend as when the samples were individually tested. This could mean that the samples do not have to be exactly the same in order for a trend between pre- and post-compression material values to be seen.

Furthermore, it could mean that regardless of the initial density (within a certain range) the behavior of the layered sample under load remains the same. This speculative conclusion has implications for the results to follow.

3. Results & Discussion

3.1. MTS Compression Testing

3.1.1. Ratcheting

205

210

The structure of near surface natural snow, even in polar regions, is more than 50% air (Salm, 1982). When loaded in compression, considerable consolidation is inevitable. As the original ice grain arrangement and intergranular bonding become stressed beyond their support limit, a rapid stress drop at a fixed strain, or collapse, occurs to create a new arrangement and intergranular contact areas (Löwe et al., 2020). An increase in stress with strain then begins anew and typically continues until snow densities reach about 0.5 where closest packing of ice grains is reached (Mellor, 1977). This is typical of confined compression testing of low to mid density snow where a ratcheting pattern is superposed on an asymptotic curve (Abele, 1990). Our high strain rate tests demonstrated this well documented behavior (Fig. 2), however, at low strain rates this behavior cannot be discerned due to insufficient sampling, a limiting feature of our MTS system.





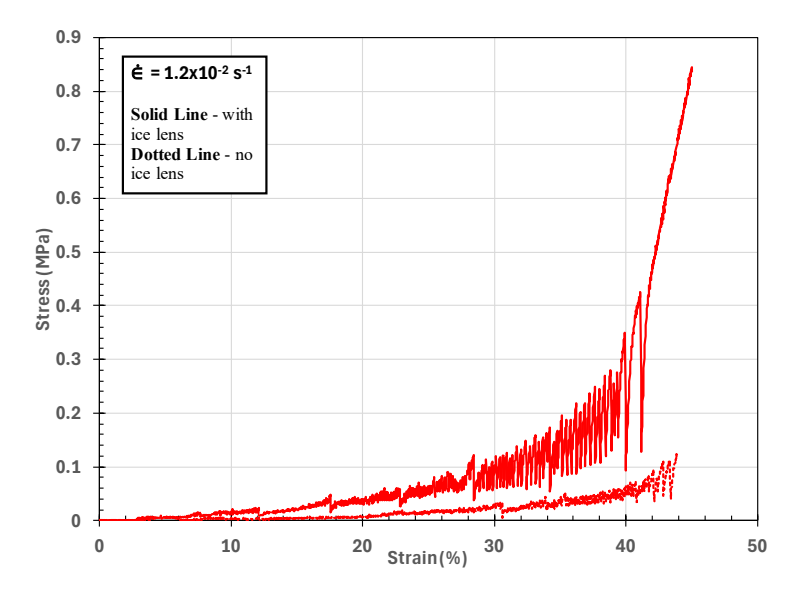


Figure 2. Ratcheting behavior can be observed throughout the test duration for high strain rates, as exemplified in this stress-strain curve for the highest strain rate tested, $1.2 \times 10^{-2} \, s^{-1}$, on aged snow.

215 3.1.2. Aged Snow

220

225

Stress-strain relationships for 8-month-old ('aged') snow columns containing an ice lens at eight strain rates are shown in Figure 3. Two types of behavior are clearly shown. In one type, a slow but gradual rise in stress accompanies increasing strain. This pattern continues all the way to 40% strain with the slope steadily increasing. This depicts a gradual stiffening of the snow sample as strain progresses. Tests showing this behavior exhibit stresses at 40% strain ranging from 1 MPa to over 3 MPa. This behavior of continuous gradual strengthening is present only for the lower strain rates from 3 x 10^{-3} s⁻¹ to 4 x 10^{-4} s⁻¹.

The second type of behavior apparent in the data is a distinct change in slope at some point as deformation progresses. This behavior is unique to the highest strain rates tested i.e., $4 \times 10^{-3} \text{ s}^{-1}$, $8 \times 10^{-3} \text{ s}^{-1}$ and $1.2 \times 10^{-2} \text{ s}^{-1}$. For these tests, the stress increases very slowly until between 15-27% strain. This increase is distinctly less than for the snow at slower strain rates. Upon reaching an 'inflection point' the samples strengthen rapidly and approximately linearly, quickly reaching stress levels at the upper levels of 2-3 MPa similar to those reached in the slower strain rate tests.

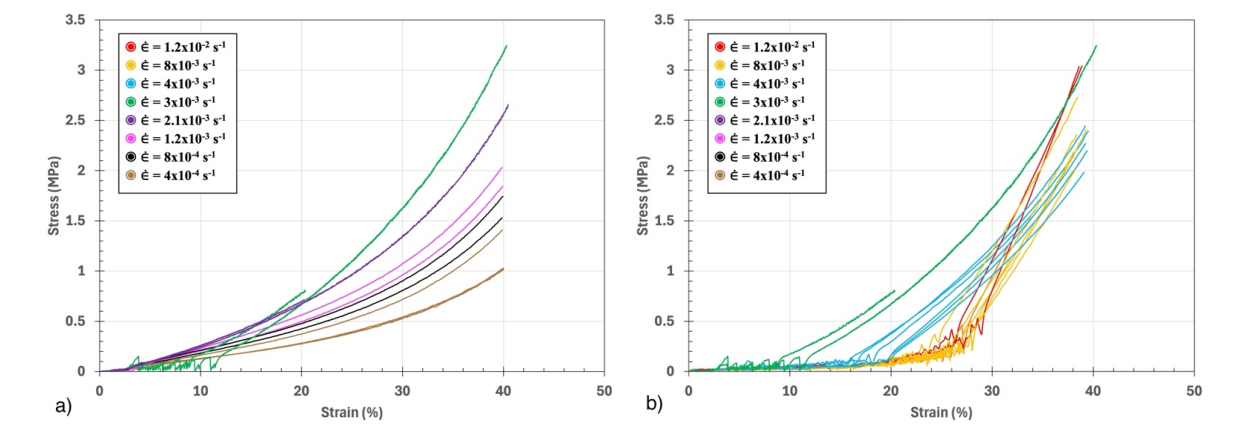






Figure 3. Stress-strain curves for all eight strain rates (low rates on left, high rates on right) tested on aged snow with an ice lens.

To characterize the behavior at each strain rate, least-squares curve-fits were generated (Fig. 4). For the slowest three strain rates, a 4^{th} -order polynomial provided a good representation of the family of curves with R^2 values more than 0.9. The midrange strain rates of $2.1 \times 10^{-3} \text{ s}^{-1}$ and $3 \times 10^{-4} \text{ s}^{-1}$ had only two replicates, and a 2^{nd} -order polynomial was adequate to achieve an R^2 of nearly 1.0.

The three highest strain rate test results were curve-fit in two parts, before (low strain) and after (high strain) the inflection point. A 3^{rd} -order polynomial was used for lower strain levels, and, once the stress began to rise rapidly, a 2^{nd} -order polynomial was fit to the data with R^2 values greater than 0.9 for all except for the lower strain regimen of 4 x 10^{-3} s⁻¹. The transition between the polynomial and approximately linear regimes of the high strain rate tests occurred at 17.5%, 26%, and 27% respectively for strain rates of 4 x 10^{-3} s⁻¹, 8 x 10^{-3} s⁻¹, and 1.2 x 10^{-2} s⁻¹.

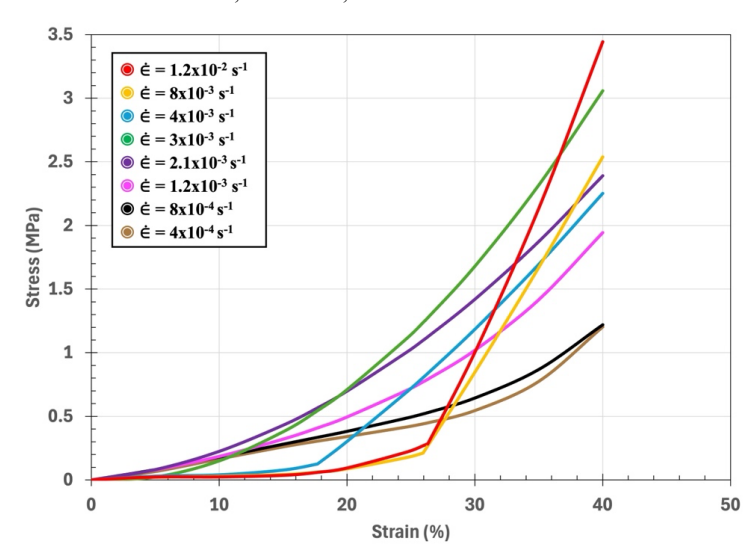


Figure 4. Trendlines for each strain rate tested on aged snow with an ice lens.

The stress at a particular strain level does not appear to be a linear function of the strain rate (Fig. 5). The data collected in this test series shows that intermediate strain rates generate the strongest snow at strain levels of 20% and 30%. Faster or slower strain rates do not reach the same level of strength as tests at 2.1 x 10⁻³ s⁻¹ or 3 x 10⁻³ s⁻¹. By the time 40% strain is reached, this pattern appears to change. While strength levels generally increase with increasing strain rate up to 3 x 10⁻³ s⁻¹, a different pattern is shown for the three highest strain rates at 40% strain. Although the final stress for strain rates 4 x 10⁻³ s⁻¹ and 8 x 10⁻³ s⁻¹ are less than for the 3 x 10⁻³ s⁻¹ tests, a steadily increasing level of stress occurs with increasing strain rates. This may be a feature of the different types of stress-strain behavior noted earlier. Indeed, Figure 4 suggests that if testing proceeded beyond 40% strain, all of the highest three strain rates would yield stresses greater than those achieved from lower strain rate testing where a different stress-strain behavior dominates.



255

260



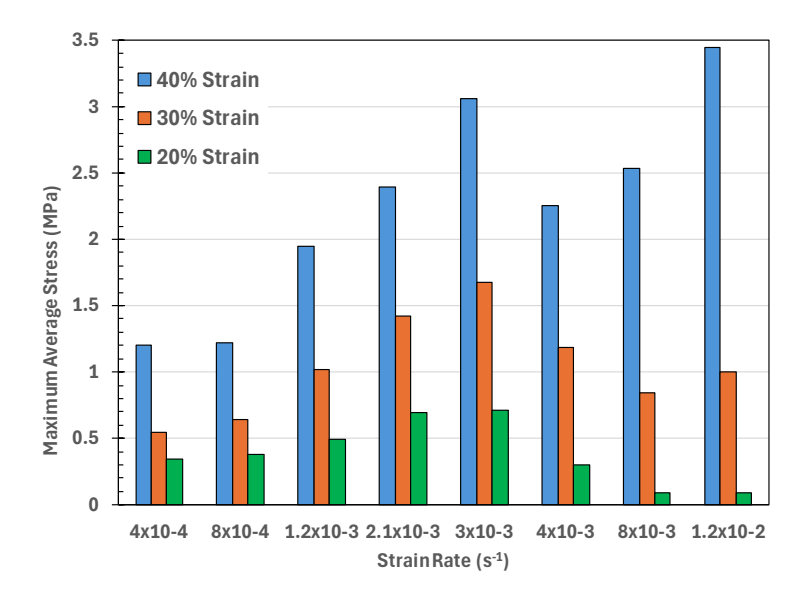


Figure 5. Trends across strain rates for tests on aged snow with an ice lens. Experimental variability can be found in the appendix.

To discern the impact of an ice lens on snow strength, tests were performed without a lens. The results are summarized in Figure 6. Little difference in stress-strain behavior can be detected at strains below about 20%. At the higher strain rates the transition between slowly and steeply rising stress with displacement occurs at a total strain about 6% sooner for snow with an ice lens. This offset appears to remain fixed as the strain progresses, suggesting that stress development is identical for snow with and without an ice lens, but that a greater total strain is required to reach a given stress if a lens isn't present.

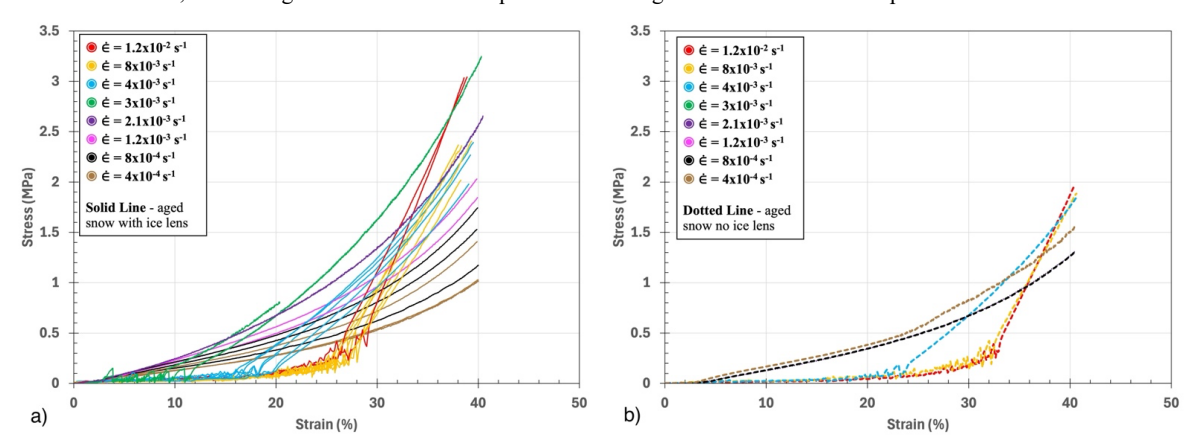


Figure 6. Lens (left) versus no lens (right) behavior of aged snow.

The difference between tests at lower strain rates is not as obvious but generally follows the trend seen in high rates: samples without a lens yielded lower overall strengths compared to samples with a lens. Combining the lens vs. no lens results over the range of strain rates tested, we conclude that the presence of an ice lens increasingly stiffens a column of snow in compression as the strain rate increases. Although the shape of the stress-strain curve remains identical for tests with and without an ice lens for all strain rates, the compressive displacement needed to reach a given strength level ranges from about 6% less when an ice lens is present at the highest strain rate to no difference at the lowest strain rate.

3.1.3. Fresh Snow



275

280



Although no test repeat tests were performed for fresh snow due to limited availability, side-by-side comparisons of aged versus fresh snow and comparisons of fresh snow with and without an ice lens were completed as a complement to the more exhaustive study with aged snow. Remarkably, nearly all the observations made for the aged snow are identical to those made on the on the fresh snow (Fig. 6 versus Fig. 7).

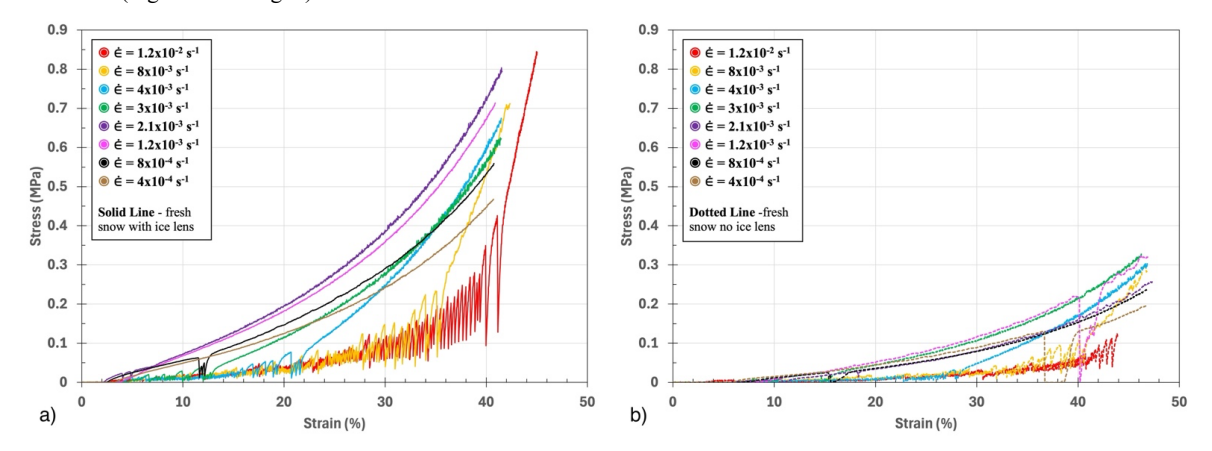


Figure 7. Lens (left) versus no lens (right) behavior of fresh snow.

As with the aged snow, the fresh snow exhibited two types of behavior for high strain rates, transitioning at an inflection point from a slowly increasing polynomial to a steeply sloped linear curve. The singular difference between aged and fresh are the stress levels reached; fresh snow yielded less than half the strength of older snow at essentially all strain states. The lower stress for any given strain was consistent for all strain rates, yet the shapes of the stress-strain curves are nearly identical. This indicates that, regardless of snow age, variations in strain rate produce the same stress-strain response but with varying magnitudes.

Similarly, the relationship of results for fresh and aged snow with or without an ice lens are nearly identical. Thus, the presence of an ice lens greatly increases the ability of a snow column to resist compaction, no matter the age of the snow grains. Further, both fresh and aged snow show similar response to different strain rates during compression. While the magnitude of stress for aged versus new snow differs greatly, up to about 35% total strain intermediate strain rates consistently yield the strongest snow. However, beyond about 35% total strain, the highest strain rates ultimately produce the strongest snow.

A significant difference is seen when comparing fresh versus aged (Fig. 8) and lens versus no lens (Fig. 7). For fresh snow, as was true for aged snow, the strength levels reached for snow columns with no ice lens are considerably less than when the lens is present. For both fresh and aged, the presence of an ice lens strengthens the snow column by a factor of 2 to 3. However, for both lens and no-lens cases, aged snow shows a remarkably higher strength, about six times that of fresh snow.





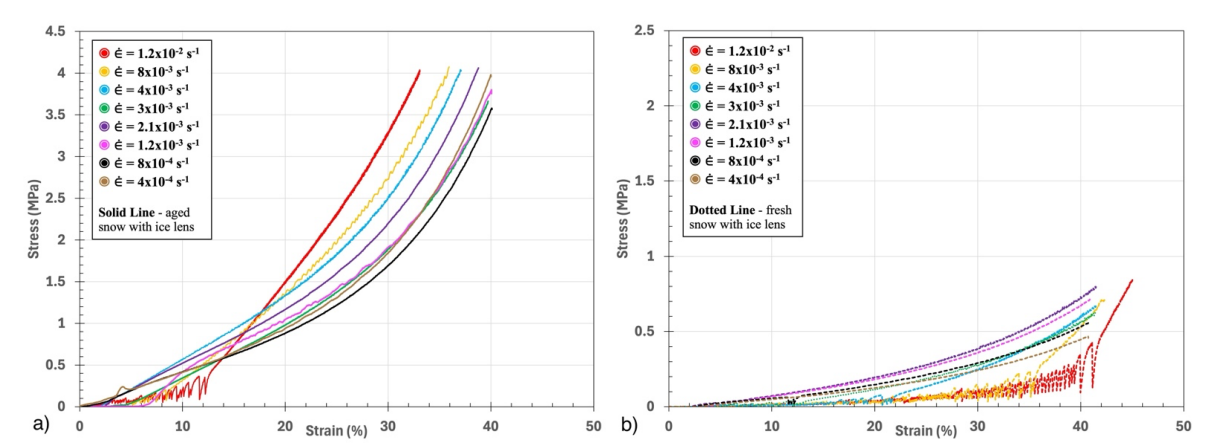


Figure 8. Comparison of response to compression for aged (left) and fresh (right) snow with an ice lens. Note the difference in scale between the plots.

3.2. Microstructural Observations

The MicroCT yielded important qualitative information about the progression of grain movement and bonding at varying rates of loading. Visual differences between pre- and post-compaction are significant (Fig. 9). For all rates of loading, the grain packing or spacing increased with compaction, but the visual differences between strained samples was difficult to discern. However, analyzing the connectivity density and specific surface area revealed a trend at intermediate rates (Fig. 10).

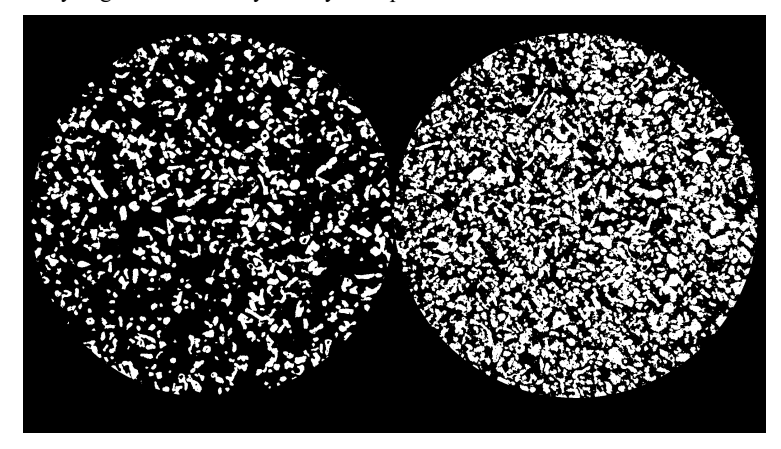


Figure 9. MicroCT binary images of aged snow with an ice lens before (left) and after (right) compaction. The compacted sample was strained at 1.2×10^{-2} s⁻¹. The snow is white and the air is black.



300

305

315

320



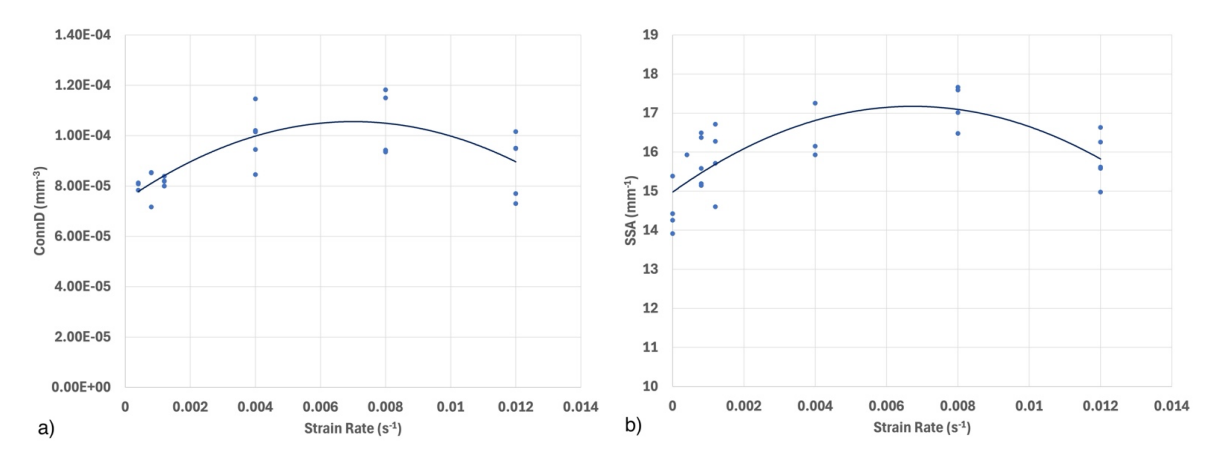


Figure 10. Plots of connectivity density (left), and specific surface area (right) for aged samples with an ice lens strained to 20%.

There were fewer test replicates of the MicroCT data due to time and equipment constraints. Due to these limitations, only tests of aged snow with an ice lens were analyzed with the MicroCT. While unable to comprehensively compare samples with and without an ice lens, and between samples of fresh and aged snow, trends are seen in the available data. There was discernable scatter between samples of the same strain rate, a result of the inherent variability in sample preparation and small changes in microstructure from exposure to room temperature air during the short walking distance between the MTS and MicroCT cold rooms. Given these caveats, connectivity density and specific surface area show polynomial trendlines with minima at the extremes and maxima in the intermediate-rate zone. Representing the frequency of bonds between ice particles and the magnitude of structural metamorphosis respectively, these variables both corroborate the MTS finding that intermediate strain rates result in larger stresses (greater strength) than high and low rates. The strengthening of the snow can explain the increase in ConnD and SSA.

3.3. Discussion

In analyzing the MTS data, four primary observations can be articulated. The first and second can be seen by comparing the two main variables in this work, the presence of an ice lens and the age of the snow. The third and fourth are true for all test cases – aged snow with an ice lens, aged snow without an ice lens, fresh snow with an ice lens, and fresh snow without an ice lens– and can be explained with both MTS and MicroCT data.

The first observation is apparent by comparing tests with and without an ice lens. For both aged and fresh snow, the presence of an ice lens requires higher stresses to reach a given total strain (Figs. 7 and 8). The difference in stresses between samples compressed with and without a lens is increased with increasing total strain.

For both aged and new snow, the presence of an ice lens increased the stress level at any given strain by 3 to 4 times. While this is certainly significant, it is possible that in a field setting the difference may be less, or even undetectable. In our tests, the relative depth of the ice lens compared to the height of the pressure bulb developed under concentrated loading was at a higher ratio compared to what may occur in a deep snowpack. Additionally, our tests involved a confined column of snow whereas loading in a field situation is more typically unconfined.

As has been observed by others (e.g., Abele, 1990), the progression of compaction can be described in distinct steps. Collapse and densification of a snow layer directly under the loading piston occurs first until that layer has adequate strength to allow the next deeper layer of snow to be loaded. Visual observation of this process has been described by Eppanapelli (2019) and



325

335

340

345

350

355

360



Barraclough (2017). In these studies, the progression of compaction is seen to be noncontinuous by using DVC and DIC methods to visualize strain and displacement fronts. In applying these results to our study, for samples containing an ice lens at mid height the displacement field would not reach the lens until the upper portion had been significantly compacted. Figure 5d in Eppanapelli (2019) clearly shows this stepwise deformation progressing from the snow layer closest to the compacting piston into the height of the sample. Additionally, the physics of deformation explained by Barraclough (2017) describes compaction of homogeneous snow proceeding in a strongly heterogeneous manner: a compacted region is separated from an uncompacted region by a moving front where the strain rate concentrates. This front originates at the compacting sources before progressively engaging more of the sample's thickness. This repetition leads to a bouncing motion of deformation termed "strain oscillation". Furthermore, results indicate that a decrease in strain rate makes the bands disappear, giving way to homogeneous plastic flow (Barraclough, 2017).

Theoretically if we were to apply this result to samples containing an ice lens, this oscillation would mean that initially only the region above the lens would experience deformation, since practically the ice lens acts as a "base" from which the front reflects. After the upper region is strain saturated, the front would then push the lens downwards to allow the oscillation to progress to the lower region. This phenomenon was visually apparent for the heterogeneous compression tests in this study and moreover, the homogeneous plastic flow which arose from a decreased strain rate reported by Barraclough is seen in our results in the continuous stress-strain behavior of low strain rates (Fig. 3).

It should be mentioned that there is an apparent contradiction in the mechanical impact of the ice lens on a volume of snow. While it is true that the presence of an ice lens within a snowpack provides a sharp heterogeneity that creates an interface between the ice and snow, the strength (or lack thereof) of the interface is highly dependent on the direction and magnitude of loading. When loaded in shear, the boundary between ice lens and snow is weak, and is a known initiation mechanism for slab avalanches (Schweizer, 1999). However, this interface behaves oppositely when loaded in a direction normal to the ice lens, as seen in the results of this study. Loading in a perpendicular direction (with respect to the ice lens) produces higher stresses than a homogeneous snow sample due to the strengthening phenomena detailed earlier. Although our experiments did not include shear testing, these results are nevertheless important for understanding snowpack stability in the presence of an ice lens. From our tests it is clear that different loading conditions can produce significantly different results and thus is a crucial aspect to avalanche and snowpack stratigraphy research.

The second observation from the MTS data is that for tests both with and without an ice lens, aged snow is stronger than fresh snow (Figs. 7, 8, and 9). The phenomenon of time-induced sintering is well established. Sintering produces the adhesion of two ice surfaces in contact (Hobbs et al., 1964). The buildup of adhesion is time-dependent; the longer the particles remain in contact, the stronger the cohesive bond created (Szabo et al., 2007). However, since both fresh and aged snow was sieved into the sample containers, it is unlikely that the sintering-induced bonding associated with the aged snow explains our results. Our sintering took place in a dry, isothermal setting. In this situation, the metamorphic process primarily acts to reduce free energy of ice particles (lower SSA) rather than affect the intergranular bonding (Kaempfer et al., 2007). Reducing the SSA essentially lessens the angularity of snow's ice grains, trending toward spherical particles. It is this difference between aged and fresh snow that probably makes the former more resistant to compression (Yong et al., 1977). More rounded ice particles will become closely packed more rapidly, without the need for, and more resistant to, actual breakage of the ice grain. Thus, with a starting point of stronger individual ice grains (even at a similar density to more angular particles) it would follow that such a snow column would more quickly be able to support compressive loading.

The difference in maximum stress reached for a given strain is magnified between aged and fresh snow when an ice lens is present; aged snow with an ice lens results in stresses approximately six times larger than fresh snow with a lens (Fig. 8). Without an ice lens present, the difference in stresses between aged and fresh snow is on the order of two to three times larger (Fig. 7).



365

375

380

390



Since both the presence of an ice lens and the degree of ice particle sintering are strengthening mechanisms, the difference between aged and fresh snow is compounded by an ice lens, hence the six-fold difference compared to a lesser amount without a lens.

The third and fourth trends, which are seen across all testing scenarios, are the split trendline behavior for the high strain rate tests, and the general 'strength ranking' at increments of total strain. These can be explained by a synthesis of MTS and MicroCT data.

Intermediate rates yielded the largest stresses, consistently above high and low rates, up until approximately 30% strain, beyond which are surpassed by high strain rate samples (Fig. 5). Our results are remarkably consistent with findings reported by eet al. (2024) and Wang et al. (2021). The former describes three modes of failure during unconfined compression testing of natural snow at various fixed loading rates: ductile, brittle, and transitional. Zheng et al. (2024) place peak snow strength between strain rates of 3 x 10⁻³ s⁻¹ and 7.6 x 10⁻³ s⁻¹, stating that rates below 1.5 x 10⁻³ s⁻¹ show ductile behavior (continuously increasing stress-strain curves) while those greater than 7.6 x 10⁻³ s⁻¹ display brittle failure (an abrupt change in stress-strain behavior). These modes of behavior are seen in our data (Fig. 4) with peaks occurring in the same range (Fig. 5). This result shows that the same failure modes seen in homogeneous snow columns are also present in the heterogeneous samples and furthermore, that a certain level of heterogeneity, in this case an ice lens, does not change the quasi-plastic behavior seen in homogeneous snow columns. However, future work should be conducted in order to understand the full impact of an ice lens on these failure modes.

MicroCT analysis also supports the MTS results; snow strength rises then falls with increasing strain rate. Specifically, Connectivity Density and Specific Surface Area show maxima tended to skew towards intermediate rates of loading. The frequency of bonding, or number of connections, between ice crystals determines the magnitude of stress the snow can generate (Wang and Baker, 2013).

Since pressure sintering stimulates accelerated bonding (Montmollin, 1982), a loading environment which allows time for bonds to form but not to a degree that impedes tight packing of ice grains would seem to lead to maximum resistance to compressive loading. This maximum would occur when the rate of loading both prevents mass failure and promotes bond growth, resulting in a large number of bonds. At these rates, the creation of new bonds and growth of existing bonds is fast enough to avoid stress accumulation yet strengthen the connections through pressure sintering. The degree of metamorphosis as quantified by SSA is maximum at high stresses (occurring at intermediate rates) because of the same phenomena; fast evolution of the bond system results in a highly complex structure which offsets the increase in stress with an increase in dimensions. These results affirm the MTS finding that intermediate rates yield maximum stresses at mid to high total strains.

Finally, the majority of avalanche crack propagation studies are centered around depth or surface hoar as the weak layer, or use a generalized heterogeneous snowpack for modeling, while the specific role of the ice-snow interface that occurs with buried ice lenses does not appear to have the same attention. This study highlights the significant effect that ice lenses can have on snow's mechanical and microstructural properties. While this research was focused on compressive loading tests which may not have direct applicability to avalanche modeling, the prospect of a weak layer that may propagate cracks differently than depth hoar is crucial to address in order to increase the accuracy of these models.

4. Conclusions

Confined compression tests were performed on both aged and fresh -10°C snow columns. Uniform samples were prepared both with and without a 2 mm manufactured ice lens at its midpoint aligned perpendicular to the loading direction. Test repetitions were completed at eight strain rates ranging from 4×10^{-4} to 1.2×10^{-2} s⁻¹. Using displacement rate as a control, resistance to loading



405



was measured, allowing the stress-strain behavior of samples to be characterized continuously to 40% strain. Microstructural analysis was also performed on some of the snow samples both before and after compression.

We found that the presence of an ice lens in both aged and fresh snow allowed the snow to support three to four times greater stress for the same level of strain. Additionally, aged snow samples, with or without an ice lens, were approximately six times more resistant to compression than fresh snow. The effect of strain rate showed pronounced differences in stress-strain behavior for all samples tested. For any given sample type (aged vs fresh; with or without ice lens), intermediate strain rates yielded the largest stresses, consistently above higher and lower rates, up to approximately 30% strain. MicroCT analysis also supported this finding; Connectivity Density and Specific Surface Area show maxima that coincide with intermediate rates of loading. Finally, we noted a distinct change in stress-strain behavior associated with high and low strain rates. Tests at low strain rates (4 x 10^{-4} to $1.2 \times 10^{-3} \text{ s}^{-1}$) showed a slow but gradual rise in stress with increasing strain. At high strain rates (4 x 10^{-3} to $1.2 \times 10^{-2} \text{ s}^{-1}$), a distinct change in slope occurred as deformation progressed; stress increased very slowly until ~20% strain whereupon stress rose rapidly and linearly. Furthermore, the failure modes and snow behavior well-established in the literature for homogeneous snow columns (Hagenmuller et al., 2015; Montmollin, 1982; Löwe et al., 2020) appears to be true for snow containing an ice lens (at a perpendicular direction to loading). This can offer insight as to how a layered snowpack may behave under varying loads.

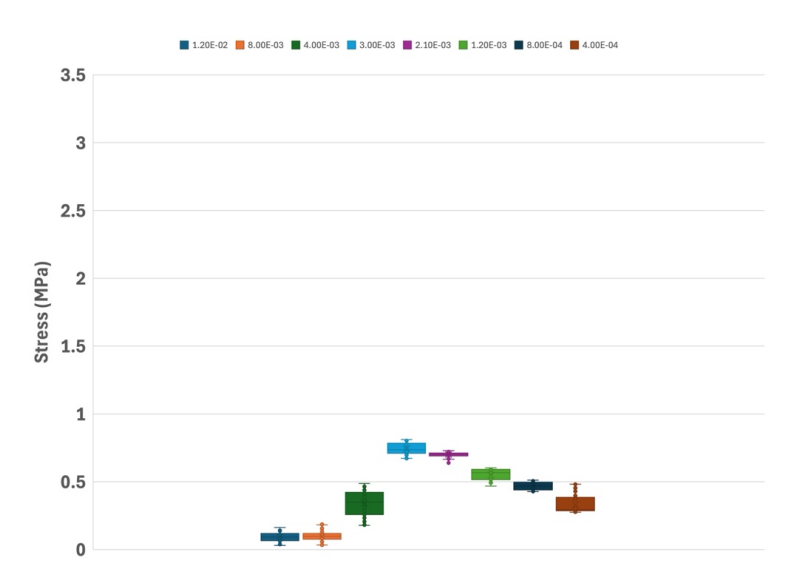
From our analysis it appears that grain slippage occurs at high strain rates and, to a lesser extent, low strain rates. Ice grain bonding is maximized when there is both enough time for the grains to initiate bonding and enough external force to create adequate contact pointes between the grains. It follows that the combination of a balanced amount of pressure sintering and minimal bond-fracturing, or non-rapid reconfiguration, contributes to high strength.



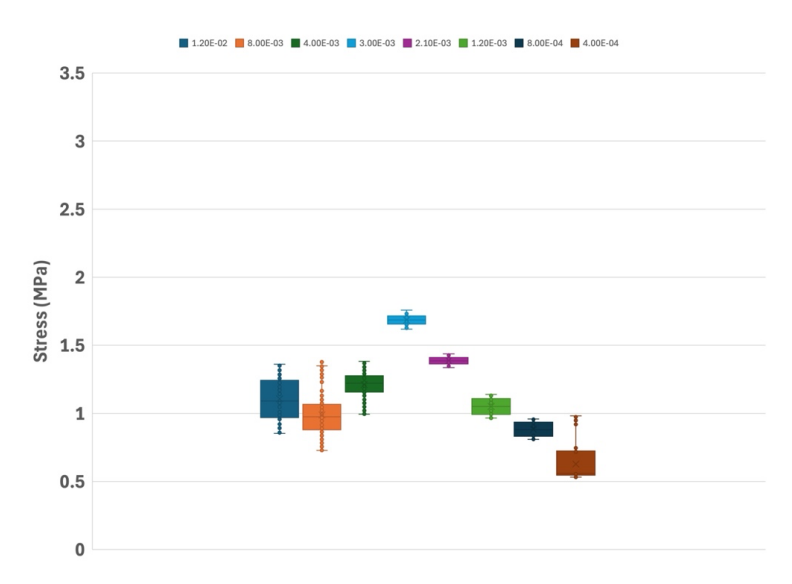


Appendix

420



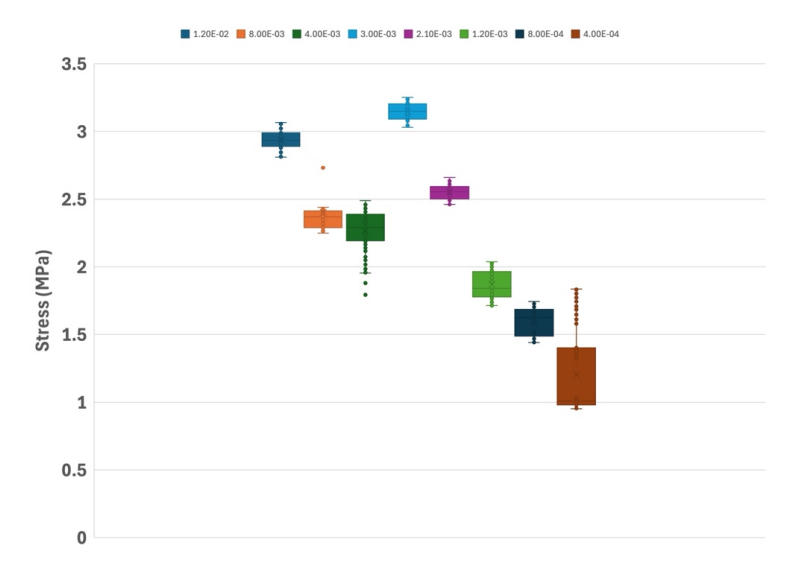
A.1. Variability of tests of aged snow with an ice lens at 20% strain.



425 A.2. Variability of tests of aged snow with an ice lens at 30% strain.







A.3. Variability of tests of aged snow with an ice lens at 40% strain.

430 *Code and Data Availability.* The data that supports the plots within this paper and other findings of this study are available from the corresponding author upon request.

Author Contributions. IB and MnB designed the study. IB provided funding and direction to the project. MnB collected snow, carried out the laboratory tests, and analyzed data. MnB and IB wrote the manuscript. All authors contributed to the paper.

Competing Interests. The authors declare that they have no conflict of interest.

435 Acknowledgements. This research was supported by NSF grant 2227842. The use of the Ice Research Laboratory (Director Professor E.M. Schulson) is gratefully acknowledged. We would like to mention Andrii Murza, the Dartmouth Ice Research Laboratory Manager, for assisting in the operation and maintenance of equipment used in this study.





References

- 440 Abele, G. Snow roads and runways. CRREL Monograph. 90(3). 1990.
 - Baker, I. Microstructural characterization of snow, firn and ice. *Philosophical Transactions of the Royal Society A*. 377(2146). 2019. doi:10.1098/rsta.2018.0162
 - Barraclough, T.W., Blackford, J.R., Liebenstein, S., Sandfeld, S., Stratford, T.J., Weinländer, G. and Zaiser, M. Propagating compaction bands in confined compression of snow. *Nature Physics*. 13. 2017. doi:10.1038/NPHYS3966
- Cohen, J., Ye, H. and Jones, J. Trends and variability in rain-on-snow events. *Geophysical Research Letters*. 42. 2015. doi:10.1002/2015GL065320
 - De Biagi, V., Barbero, M., Barpi, F., Borri-Brunetto, M. and Podolskiy, E. Failure mechanics of snow layers through image analysis. *European Journal of Mechanics/A Solids*. 74. 2019. doi:10.1016/j.euromechsol.2018.10.018
- Eppanapelli, L.K., Forsberg, F., Casselgren, J. and Lycksam, H. 3D analysis of deformation and porosity of dry natural snow during compaction. *Materials*. 12. 2019. doi:10.3390/ma12060850
 - Gaume, J., Chambon, G., Eckert, N., and Naaim, M. Influence of weak-layer heterogeneity on snow slab avalanche release: application to the evaluation of avalanche release depths. *Journal of Glaciology*. 59(215). 2013. doi:10.3189/2013JoG12J161
- Gunderson, H.J.G., Boyce, R.W., Nyengaard, J.R., Odgaard, A. The Conneulor: unbiased estimation of connectivity using physical dissectors under projection. *Bone*. 14, 217-222. 1993.
 - Hagenmuller, P. Snow mechanics: from snow microstructure to avalanche formation. *Glaciology*. Université Grenoble Alpes, 2022. HAL Id:tel-04143903
 - Hagenmuller, P., Chambon, G. and Naaim, M. Microstructure-based modeling of snow mechanics: a discrete element approach. *The Cryosphere*. 9(5). 2015. doi:10.5194/tc-9-1969-2015
- 460 Hagenmuller, P., Theile, T. and Schneebeli, M. Numerical simulation of microstructural damage and tensile strength of snow.
 Geophysical Research Letters. 41(1). 2014c. doi:10. 1002/2013GL058078
 - Hammonds, K., Lieb-Lappen, R., Baker, I. and Wang, X. Investigating the thermophysical properties of the ice-snow interface under a controlled temperature gradient. *Cold Regions Science and Technology*. 120. 2015. doi:10.1016/j.coldregions.2015.09.006
- 465 Hobbs, P. V., and B. J. Mason. The Sintering and Adhesion of Ice. *Philosophical Magazine* 9(98), 181–97. 1964. doi:10.1080/14786436408229184
 - Jamieson, B. Formation of refrozen snowpack layers and their role in slab avalanche release. *Review of Geophysics*. 44(2). 2006. doi:10.1029/2005RG000176
- Kaempfer, T. and Schneebeli, M. Observation of isothermal metamorphism of new snow and interpretation as a sintering process. *Journal of Geophysical Research: Atmospheres*. 2007. doi:10.1029/2007JD009047
 - Kockhle, B. and Schneebeli, M. Three-dimensional microstructure and numerical calculation of elastic properties of alpine snow with a focus on weak layers. *Journal of Glaciology*. 60(222). 2014. doi:10.3189/2014JoG13J220





495

- LaChapelle, E. Secrets of the snow: visual clues to avalanche and ski conditions. University of Washington Press. 2011.
- LaChapelle, E. Snow avalanches: a review of current research and applications. *Journal of Glaciology*. 19(81). 1977. doi:10.3189/S0022143000215633
- Löwe, H., M. Zaiser, S. Mösinger, and S. Schleef. Snow Mechanics Near the Ductile-Brittle Transition: Compressive Stick-Slip and Snow Microquakes. *Geophysical Research Letters*. 47(4) 2020. doi:10.1029/2019gl085491
- Ma, C., Zheng, H., Yang, N., Sun, T., Si, J., and Ren, D. Microstructural evolution and mechanical properties of snow under compression. *Construction and Building Materials*. 472. 2025. doi:10.1016/j.conbuildmat.2025.140883
- 480 Magono C. and Lee C.W. Meteorological Classification of Natural Snow Crystals. Journal of the Faculty of Science, Hokkaidô University, Japan. 2(4). 1966.
 - Mellor, M. Engineering properties of snow. Journal of Glaciology. 19(81). 1977.
 - Montmollin, Vincent De. Shear Test on Snow Explained by Fast Metamorphism. *Journal of Glaciology*. 28(98), 187–98. 1982. doi:10.3189/s0022143000011898
- 485 Odgaard, A. Three-dimensional methods for quantification of cancellous bone architecture. Bone. 20(6), 315-328. 1997.
 - Queno, L., Fierz, C., van Herwijnen, A., Longridge, D. and Wever, N. Deep ice layer formation in an alpine snowpack: monitoring and modeling. *The Cryosphere*. 14(10). 2020. doi:10.5194/tc-14-3449-2020
 - Rosendahl, P.L. and Weibgraeber, P. Modeling snow slab avalanches caused by weak-layer failure Part 1: Slabs on compliant and collapsible weak layers. *The Cryosphere*. 14(1). 2020. doi:10.5194/tc-14-115-2020
- 490 Salm, B. Mechanical properties of snow. Reviews of Geophysics and Space Physics. 20(1). 1982.
 - Salmon, P. Morphometric Parameters in CT Analyser. 2009.
 - Schweizer, J. The influence of the layered character of a snow cover on the triggering of slab avalanches. *Annals of Glaciology*. 18. 1993. doi:10.3189/S0260305500011496
 - Schweizer, J. Review of dry snow slab avalanche release. *Cold Regions Science and Technology*. 30(1-3). 1999. doi:10.1016/S0165-232X(99)00025-7
 - Schweizer, J., Jamieson, J., and Schneebeli, M. Snow avalanche formation. *Review of Geophysics*. 41(4). 2003. doi:10.1029/2002RG000123
 - Szabo, D., and Schneebeli, M. Subsecond Sintering of Ice. Applied Physics Letters 90(15). 2007. doi.org:10.1063/1.2721391
- Thumlert, S., and Jamieson, B. Stress measurements from common snow slope stability tests. *Cold Regions Science and* Technology. 110. 2015. doi:10.1016/j.coldregions.2014.11.005
 - Wang, E., Fu, X., Han, H., Liu, X., Xiao, Y., and Leng, Y. Study of mechanical properties of compacted snow under uniaxial compressing and analysis of influencing factors. *Cold Regions Science and Technology*. 182. 2021. doi:10.1016/j.coldregions.2020.103215
- Wang, X. and Baker, I. Observation of the microstructural evolution of snow under uniaxial compression using x-ray computed microtomography. *Journal of Geophysical Research: Atmospheres.* 118. 2013. doi:10.1002/2013JD020352





- Wang, X., and Baker, I. Evolution of the Specific Surface Area of Snow during High-temperature Gradient Metamorphism. *Journal of Geophysical Research: Atmospheres* 119(24). 2014. doi.org:10.1002/2014jd022131
- Xiao, E. Huo, H., Dai, X., Hu, B., Li, T., Ding, J., and Tang, X. Load-bearing tests and simulation of compacted loose snow. *Construction and Building Materials*. 421. 2024. doi:10.1016/j.conbuildmat.2024.135681
- Yong, R. and Fukue, M. Performance of snow in confined compression. *Journal of Terramechanics*. 14(2). 1977. doi:10.1016/0022-4898(77)90002-7
 - Zheng, Y., Shi, W., Han, Y. and Chen, T. Compressive strength of compacted snow. *Proceedings 9th International Conference on Snow Engineering*. Shanghai, China, 3-5 June 2024.